# OVERACTIVATED BNIP3-DEPENDENT MITOPHAGY AS A DRIVER OF IMMOBILIZATION-INDUCED MUSCLE ATROPHY: THERAPEUTIC MECHANISM OF EXTRACORPOREAL SHOCK WAVE IN IMPROVING MYOGENIC CONTRACTURE

F. Wang[1,2,3], C.X. Zhou[1,3], T. Zhou[1,2,3], L.Y. Ni[1,3], Q.B. Zhang[1,3] and Y. Zhou[1,3,*]

[1]Department of Rehabilitation Medicine, The Second Affiliated Hospital of Anhui Medical University, 230601 Hefei, Anhui, China
[2]Department of Rehabilitation Medicine, The Second Affiliated Hospital of Wannan Medical College, 241000 Wuhu, Anhui, China
[3]Research Center for Translational Medicine, The Second Affiliated Hospital of Anhui Medical University, 230601 Hefei, Anhui, China

**Abstract**

**Purpose:** The purpose of this study is to investigate the role of Bcl2/adenovirus E1B 19kDa protein-interacting protein 3 (BNIP3)-dependent mitophagy in immobilization-induced muscle atrophy and explore the potential mechanism responsible for ameliorating myogenic contracture through extracorporeal shock wave (ESW). **Methods:** A rat model of myogenic contracture was developed by immobilizing the knee joint, and muscle atrophy and mitophagy were assessed *in vivo*. Subsequently, we verified the role of mitophagy in muscle atrophy through *in vitro*. Finally, we examined the potential therapeutic effects of ESW on immobilization-induced muscle atrophy and myogenic contracture, and assessed the role of mitophagy in the observed alleviation of symptoms. **Results:** Immobilization had significant time-dependent effects on muscle atrophy. It triggered the production of excessive reactive oxygen species (ROS) and subsequently overactivated hypoxia-inducible factor (HIF)-1$\alpha$/BNIP3-dependent mitophagy in the rectus femoris. Excessive mitophagy resulted in the elimination of mitochondria, leading to a shortage of adenosine triphosphate (ATP). As ATP homeostasis was crucial for maintaining muscle mass, the shortage of ATP resulted in reduced muscle mass and cross-sectional area, as well as slow-to-fast myofiber type transition. These findings were corroborated by an *in vitro* study that pretreatment with BNIP3 small interfering RNA (siRNA) reduced the level of BNIP3-dependent mitophagy and partially counteracted the inhibition of myogenic differentiation caused by high levels of ROS. Notably, ESW was found to suppress ROS generation, inhibit overactivated HIF-1$\alpha$/BNIP3-dependent mitophagy, and preserve mitochondrial quantity in the rectus femoris. **Conclusions:** Our findings suggest that ESW can inhibit overactivated BNIP3-dependent mitophagy in immobilized muscles, which could be one of the potential therapeutic mechanisms attenuating immobilization-induced muscle atrophy and further improving myogenic contracture.

**Keywords:** Muscle atrophy, myogenic contracture, immobilization, mitophagy, extracorporeal shock wave.

*Address for correspondence: Y. Zhou, Department of Rehabilitation Medicine, The Second Affiliated Hospital of Anhui Medical University, 230601 Hefei, Anhui, China; Research Center for Translational Medicine, The Second Affiliated Hospital of Anhui Medical University, 230601 Hefei, Anhui, China. E-mail: zhouyunanhui@sina.com.

## Introduction

In clinical practice, partial immobilization or bed rest is commonly used for the treatment of fractures, ligament injuries, and pain in older individuals. However, this treatment can lead to joint contracture (Li *et al.*, 2024). Joint contracture is influenced by two anatomical components around the joint: arthrogenic and myogenic components. Muscle atrophy and myofibrosis are critical factors in the development of myogenic contracture as they reduce muscle elasticity and increase joint stiffness (Kaneguchi *et al.*, 2017; Wang *et al.*, 2020b; Wang *et al.*, 2023a).

Immobilization-induced muscle atrophy is characterized by a reduction in muscle mass and function, including smaller myofiber size, transition of myofiber type, and an imbalance in protein synthesis and degradation processes (Park *et al.*, 2019; Wang *et al.*, 2020b). Previous research suggested that oxidative stress plays a key role in regulating protein synthesis and degradation in muscle during immobilization (Park *et al.*, 2019; Scicchitano *et al.*, 2018). Prolonged inactivity can lead to increased reactive oxygen species (ROS) generation from mitochondria in muscle fibers, and ROS-mediated oxidative stress triggers muscle atrophy during

immobilization (Bar-Shai *et al.*, 2008; Kang and Ji, 2013; Talbert *et al.*, 2013). Recent research also suggested that excessive ROS production has been found to induce overactivated mitophagy, causing cellular bioenergy deficits and eventual cell death (Qiu *et al.*, 2019; Zhu *et al.*, 2021). Previous research indicates that age-related muscle atrophy is partly due to ROS release and excessive mitochondrial degradation via mitophagy, resulting in reduced myofiber number and size (Wang *et al.*, 2020a). Previous research also showed that the worsening of muscle atrophy caused by immobilization during the initial phase of remobilization is associated with mitophagy (Wang *et al.*, 2023b). Mitophagy is a cellular process that selectively removes damaged or excess mitochondria through lysosomes. In skeletal muscle, Bcl2/adenovirus E1B 19kDa protein-interacting protein 3 (BNIP3) is expressed as a mitophagy receptor (Deval *et al.*, 2020; Oost *et al.*, 2019; Yamashita *et al.*, 2021). Research has shown that ROS increase the expression of hypoxia-inducible factor (HIF)-1 and its downstream target BNIP3. BNIP3 further interacts with microtubule-associated protein 1 light chain 3 (LC3) to initiate mitophagy (Wang *et al.*, 2022a; Wang *et al.*, 2022c). Despite previous studies suggesting immobilization boosts BNIP3 expression and activates mitophagy, the precise mechanism underlying the relationship between mitophagy and muscle atrophy has not been determined (Deval *et al*., 2020; Oost *et al.*, 2019).

There is currently a lack of safe and non-invasive medical therapies for preventing or reversing muscle atrophy. However, extracorporeal shock wave (ESW) has shown promise in various musculoskeletal disorders and tissue regeneration. Previous studies in rats have demonstrated that ESW enhances bone and muscle tissue regeneration by increasing the expression of growth factors and bone morphogenetic protein (Huang *et al.*, 2016; Zissler *et al.*, 2017). Adult skeletal muscle regeneration is primarily driven by myoblasts, which differentiate into myotubes and form myofibers. In addition to promoting myoblast proliferation and differentiation, preventing myoblast death is crucial in muscle atrophy treatment, particularly apoptosis and autophagy (Ou *et al.*, 2021; Yang *et al.*, 2020). Low-frequency electrical stimulation has been shown in an earlier study to mitigate immobilization-induced muscle atrophy in rabbits by downregulating autophagy (Liu *et al.*, 2022). Recent research also found that ESW inhibits ROS generation and autophagy in cardiac cells (Qiu *et al.*, 2021). Based on these findings, we hypothesize that excessive ROS production triggers muscle atrophy through HIF-1$\alpha$/BNIP3-dependent mitophagy, and ESW can protect against immobilization-induced muscle atrophy by inhibiting ROS-mediated HIF-1$\alpha$/BNIP3-dependent mitophagy (Fig. 1**A**).

Previous research on rabbits has shown that ESW can improve muscle atrophy caused by immobilization through promoting myogenic differentiation (MyoD) expression (Wang *et al.*, 2022b). However, the molecu-

lar mechanism underlying this treatment remains unclear. Wang *et al*. (2023a, 2023b) have also developed a rat model to conveniently simulate and preventively treat myogenic contracture and muscle atrophy. Aiming to explore the role of mitophagy in immobilization-induced muscle atrophy, we conducted this study. We examined whether ESW could help treat muscle atrophy and myogenic contracture induced by immobilization, while also exploring the role BNIP3-dependent mitophagy played in the observed improvement in symptoms.

## Materials and Methods

### Animals and Establishment of a Myogenic Contracture Model

The animal experimental protocol for this study comprised two distinct parts (Fig. 1**B**). In part a, thirty-six sprague-dawley male rats (approximately 3 months old, 200 g–250 g) were randomly assigned to six groups based on the length of immobility. In part b, based on intervention factor, thirty sprague-dawley male rats were randomized into five groups. As described in previous studies of Wang *et al*. (2023a, 2023b), the knee joint of left limb was immobilized by a shaped aluminum splint to establish the myogenic contracture animal model except for group Ctrl(a) and Ctrl(b). All rats were housed (3/cage) in a temperature-controlled, humidity-controlled, and light-controlled room. All rats were provided with ad libitum access to food and water.

### Protocol for ESW Treatment

The rats in groups ET(b) received ESW treatment. A radial shock wave equipment (Swiss DolorClast®, smart, Nyon, Switzerland) was applied twice a week in groups ET(b). According to previous protocol of Yuan *et al.* (2023), the rats received 2000 impulses at a dose of 1.5 bar and a frequency of 6 Hz, targeted at the left quadriceps femoris area (Fig. 1**C–E**). A small number of rats showed subcutaneous microhemorrhage in the quadriceps femoris area after ESW treatment, but it could be rapidly recovered by applying an ice compress (Fig. 1**F**).

### Measurement of Myogenic Contracture

The rats were euthanized by an overdose of sodium pentobarbital (120 mg/kg, intraperitoneal injection). The range of motion (ROM) of the left knee joint was evaluated both prior to and following the myotomy. We calculated the myogenic contracture induced by the muscular structures using the methodology detailed in prior studies (Wang *et al.*, 2020b; Wang *et al.*, 2023a).

### Skeletal Muscle Tissue Preparation

According to previous studies, the rectus femoris was selected as a character of skeletal muscle response to immobility (Wang *et al.*, 2020b; Wang *et al.*, 2023a; Wang *et al.*, 2023b). The laboratory scale (Wang *et al.*, 2023b) was used to measure muscle wet mass (MWM, mg), which was
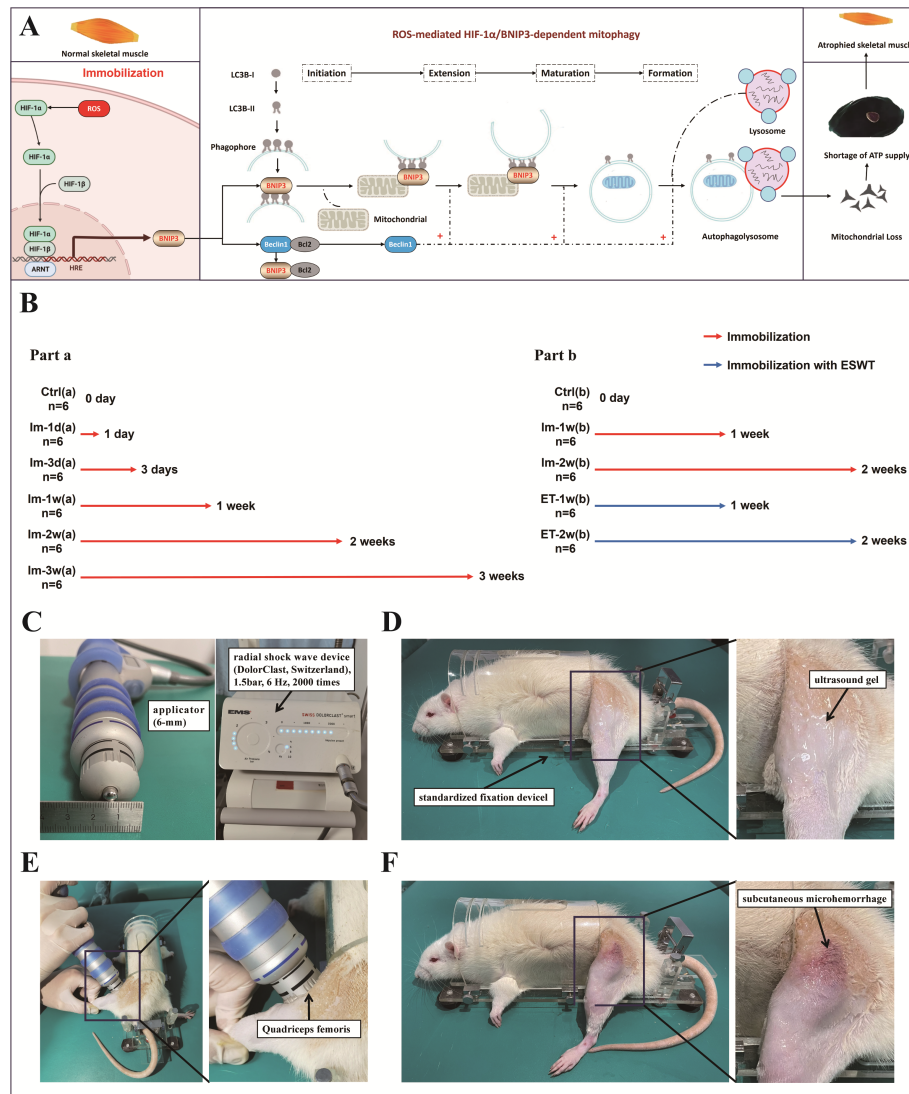
**Fig. 1. Proposed mechanisms underlying immobilization-induced muscle atrophy and the application of ESW.** (**A**) Hypothesized mechanism of muscle atrophy induced by immobilization. Immobilization leads to excessive ROS generation, which increases the transcription and translation of HIF-1$\alpha$. One receptor-dependent mitophagy pathway requires HIF-1$\alpha$-dependent expression of BNIP3. BNIP3, which binds directly to LC3B-II and mediates phagophore interactions, may impair mitochondrial function. Moreover, BNIP3 competes with Beclin-1 for Bcl-2's binding site, releasing Beclin-1 to form complexes involved in autophagosome extension, maturation, and formation. Ultimately, autophagosomes encase mitochondria and are degraded by lysosomes, leading to total adenosine triphosphate (ATP) deficiency and muscle atrophy. (**B**) Animal experimental design. (**C**) The left hindlimb was cleaned after removing the shaped aluminum splint, and the 6-mm applicator was selected in this study. (**D**) Using a standardized fixation device, the rats were fixated during the experiment to prevent anesthesia-related mistakes in the results. Then, the ultrasonic gel was evenly applied to the skin surface surrounding the quadriceps femoris of the left hindlimb. This prevented air from getting between the skin and the radial shock treatment head, which helped to reduce shock wave energy loss and preserve steady wave transmission. (**E**) To help the rats get used to the stimulation, each rat was given less than 500 shock wave impulses at a low dose of 1.0 bar, 4 Hz, to the left quadriceps femoris area. According to the instruction manual of manufacturer and our previous experimental experience, the rats were administered 2000 times impulses at a 1.5 bar, 6 Hz experimental dose to the left quadriceps femoris area. After the conclusion of each treatment, the left knee joint was immobilized again until the next treatment. At the period of ESW treatment in groups ET(b), the rats in groups Im(b) were also fixed with the standardized fixation device while the shaped aluminum splint was also removed to avoid experimental error. (**F**) A small number of rats showed subcutaneous microhemorrhage in the quadriceps femoris area after ESW treatment, but it could be rapidly recovered by applying an ice compress. ESW, extracorporeal shock wave; HIF, hypoxia-inducible factor; ROS, reactive oxygen species; BNIP3, Bcl2/adenovirus E1B 19kDa protein-interacting protein 3; ARNT, aryl hydrocarbon receptor nuclear translocator; HRE, hypoxia response element; ESWT, extracorporeal shock wave therapy.
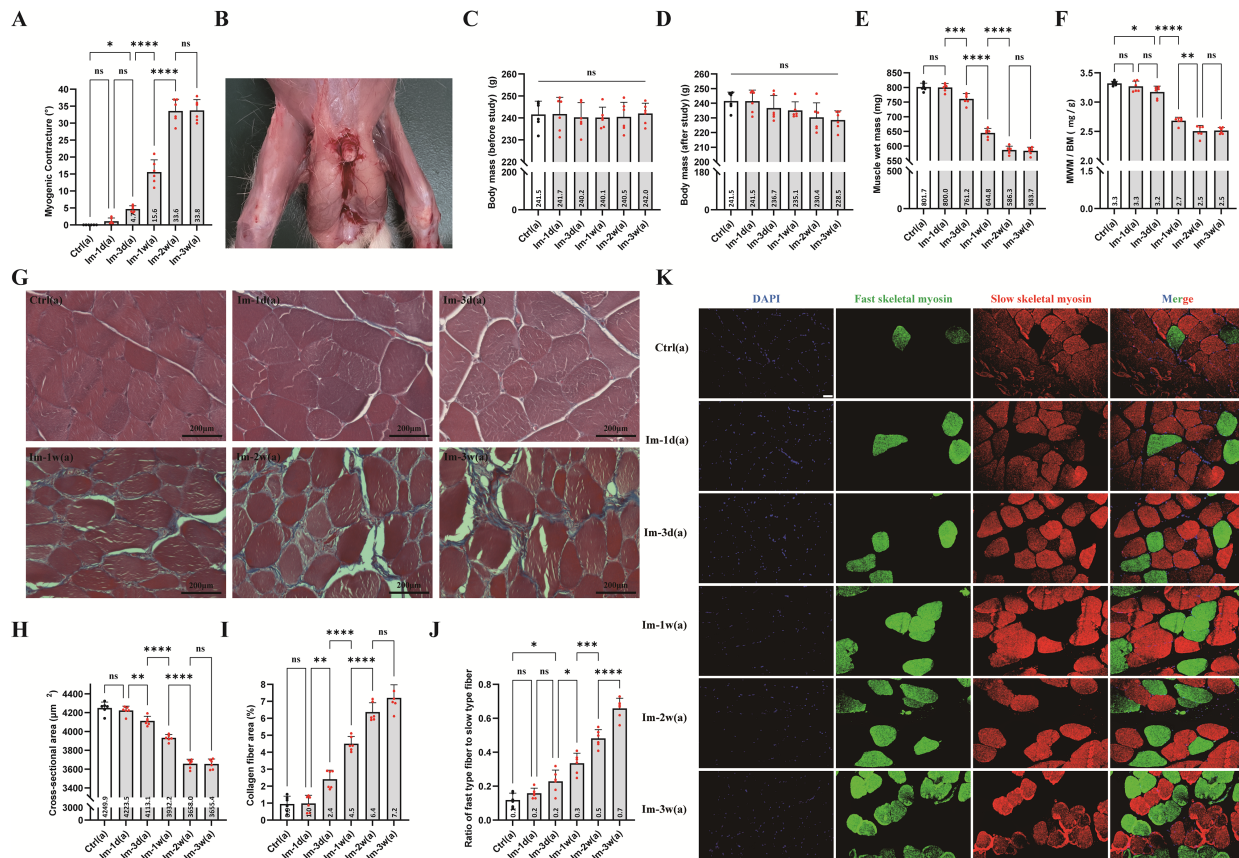
**Fig. 2. Immobilization caused myogenic contracture and muscle atrophy.** (A) Statistical graphs of myogenic contracture (°) (n = 6 per group). (B) Macroscopic muscle atrophy of the quadriceps femoris after three weeks of immobilization. (C–F) Statistical graphs of body mass (before study) (g), body mass (after study) (g), muscle wet mass of the rectus femoris (mg), and MWM/BM (mg/g) (n = 6 per group). (G) Typical Masson staining images. Scale bars = 200 $\mu$m. (H,I) Statistical graphs of cross-sectional area ($\mu$m$^2$), ratio of collagen fiber area to myofiber area (n = 6 per group). (J) Statistical graphs of calculation of the ratio of fast-twitch to slow-twitch muscle fibers (n = 6 per group). (K) Immunofluorescence assay was used to localize the expression of slow skeletal myosin (red) and fast skeletal myosin (green), with nuclei marked with DAPI (blue). Scale bars = 50 $\mu$m. All values were presented as mean $\pm$ SD. ns, no significance. \*$p < 0.05$, \*\*$p < 0.01$, \*\*\*$p < 0.001$, \*\*\*\*$p < 0.0001$. MWM/BM, the ratio of muscle wet mass to body mass; SD, standard deviation; DAPI, 4',6-diamidino-2-phenylindole.

then represented as the ratio of muscle wet mass to body mass (MWM/BM, mg/g), as well as in absolute terms. Tissue samples were taken from the mid-region of the rectus femoris, rapidly frozen in isopentane chilled with dry ice, and subsequently stored at –80 °C in a freezer.

*Masson Staining*

As previously mentioned, Masson staining was conducted utilizing a commercially available kit (Solarbio, G1340, Beijing, China) (Wang *et al.*, 2023a). Images of the rectus femoris cross-section were captured at $400\times$ magnification using an inverted phase-contrast microscope (Nikon Ltd., TE2000-U, Tokyo, Japan). Subsequently, according to previous studies, Image J software (Image J v1.46a, National Institutes of Health, Bethesda, MD, USA) was utilized to estimate the cross-sectional area (CSA) as well as the ratio of collagen fiber area to myofiber area (Wang *et al.*, 2020b; Wang *et al.*, 2023a; Wang *et al.*,

2023b). There were six fields of view examined in each section at random.

*Imaging of Transmission Electron Microscope*

After preparation, the muscle blocks were instantly immersed in 2.5 % glutaraldehyde. Coronal slices of 1 mm thick were sliced at 4 °C after 6 to 8 h. The samples were then postfixed for 1–2 h with osmium tetroxide following a rinse with phosphate buffered saline (PBS) (0.1 M). A graded series of ethanol and acetone solutions were applied to dehydrate the muscle coronal slices. Before slicing the ultra-thin sections, we embedded the sections in epoxy resin. The next step was double staining with lead citrate and uranyl acetate. Ultimately, images were obtained using a transmission electron microscope (TEM) (JEOL Ltd., JEM-1400, Tokyo, Japan). For each section, six random, noncontiguous microscopic fields were examined.
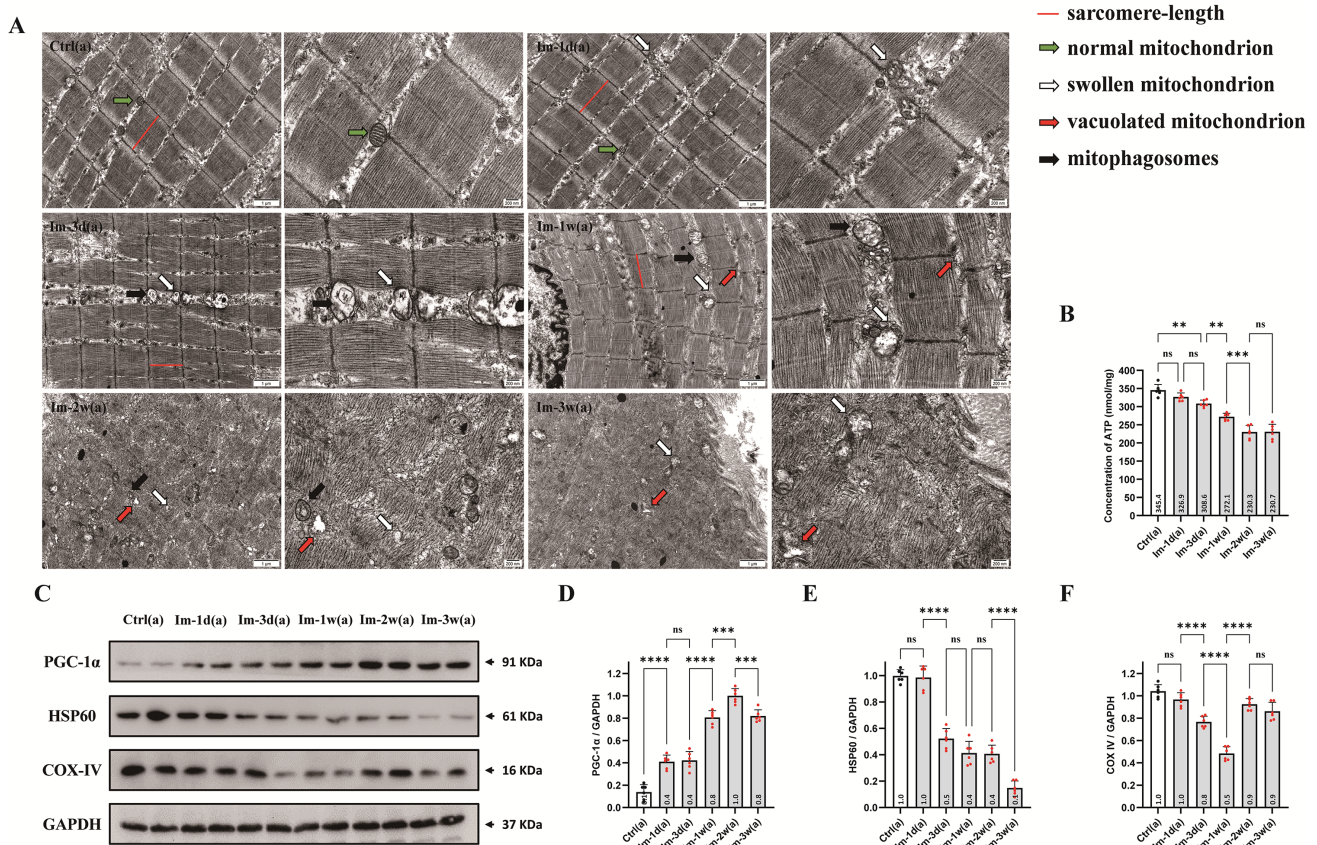
**Fig. 3. Mitophagy in skeletal muscle was overactivated after immobilization.** (**A**) Typical transmission electron microscope images (n = 6 per group). Scale bars (under a 20,000× magnification field) = 1 $\mu$m, scale bars (under a 50,000× magnification field) = 200 nm. (**B**) Statistical graphs of ATP level (nmol/mg) (n = 6 per group). (**C**) Western blotting results showing PGC-1$\alpha$, HSP60 and COX IV changes during immobilization. (**D–F**) Statistics for the grey value analysis of western blotting bands for PGC-1$\alpha$, HSP60 and COX IV (n = 6 per group). All values were presented as mean $\pm$ SD. ns, no significance. \*\*$p < 0.01$, \*\*\*$p < 0.001$, \*\*\*\*$p < 0.0001$. GAPDH, Glyceraldehyde-3-phosphate Dehydrogenase.

*ATP Assessment*

According to previous research, the content of ATP was measured using an Assay Kit (Beyotime, S0026, Shanghai, China) (Wang *et al.*, 2023b). In the end, the ATP concentrations were shown as nanomoles per milligram. Each sample was analyzed in triplicate and each ATP assessment was repeated three times. The acquired values were averaged for statistical analysis.

*Detection of ROS*

Dihydroethidium (DHE) has been used as a fluorescent indicator of ROS production in a previous study (Wang *et al.*, 2023b). Red light was detected using a fluorescence microscope (Olympus, Tokyo, Japan, BX-51) equipped with a rhodamine filter (excitation 490 nm, emission 590 nm). The thin frozen sections were incubated with 0.1 % DHE (Beyotime, Shanghai, S0063, China) for 30 min at 37 °C in a dark box, rinsed in PBS and viewed under a 400× magnification field using a fluorescent microscope (filter with excitation at 545 nm). Image J software (Image J v1.46a, National Institutes of Health, Bethesda, MD,

USA) was used to analyze six images per section for densitometry, which is expressed as a percentage, respectively, of group Ctrl(a) and group Ctrl(b).

Superoxide dismutase (SOD), for example, is a ROS scavenger that can be destroyed by excessive ROS production. As a result, SOD can be commonly used to indirectly evaluate ROS levels. The commercial kit (Nanjing Jiancheng Bioengineering Institute, A001-3, Nanjing, China) was used to measure the SOD activity in the previous study (Wang *et al.*, 2023b). Ultimately, the activity of SOD was presented as units per milligram. Each sample was processed in triplicate and each SOD detection was repeated three times independently. Mean value for each group was selected for statistical analysis.

*Immunofluorescence*

We fixed thin frozen rectus femoris sections with 4 % paraformaldehyde for 1 h and blocked nonspecific binding sites using 10 % goat serum. The slides were then incubated at 37 °C for 2 h with two primary antibodies, mouse monoclonal antibody against slow skeletal myosin
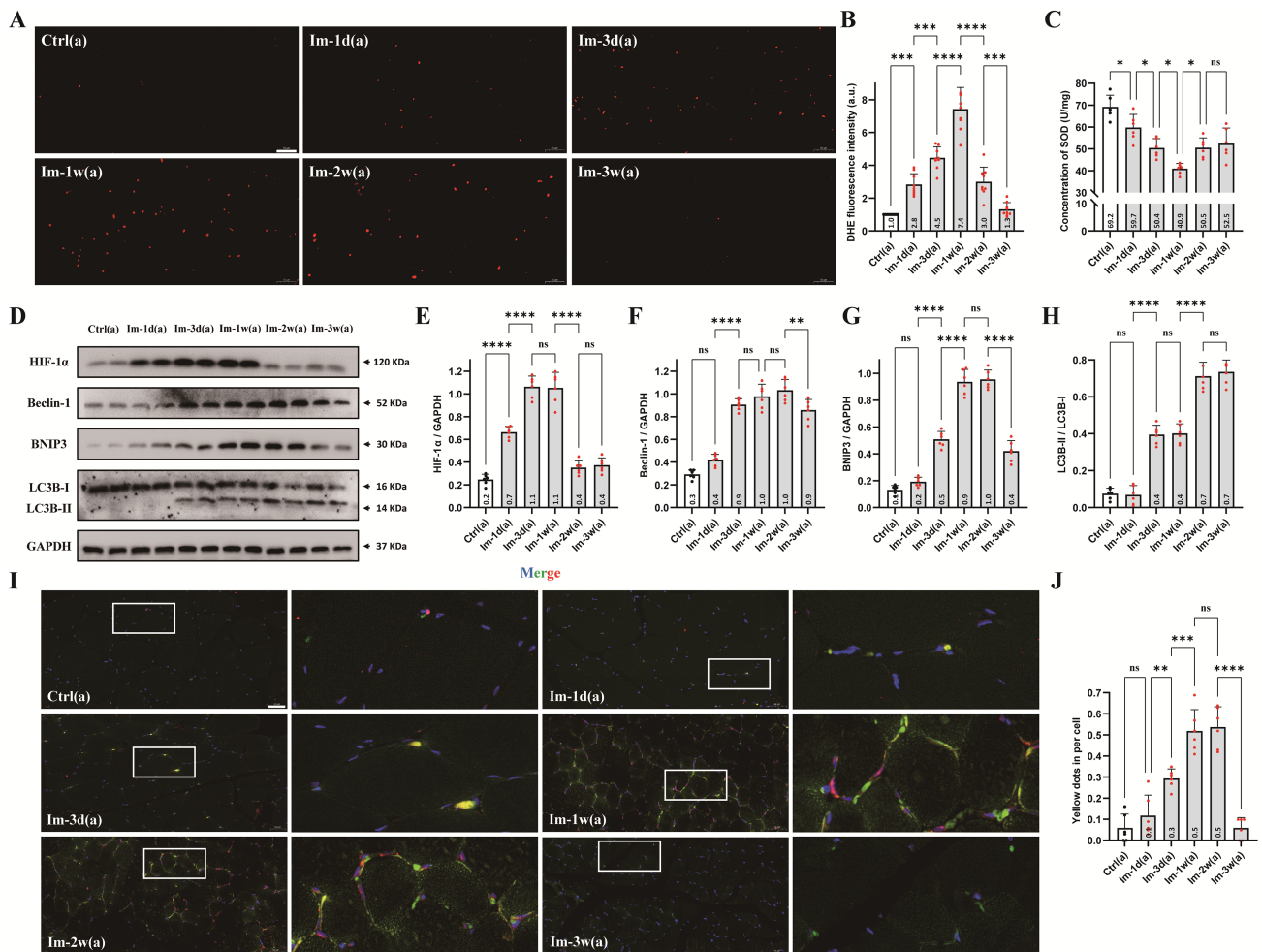
**Fig. 4. Immobilization increased ROS generation and up-regulated HIF-1α/BNIP3 dependent mitophagy.** (**A**) Typical DHE fluorescence images to assess ROS generation. Scale bars = 50 μm. (**B**) DHE fluorescence intensity in each group was described as a percentage of group Ctrl(a) (n = 6 per group). (**C**) Statistical graphs of SOD level (U/mg) (n = 6 per group). (**D**) Western blotting results showing HIF-1α, Beclin-1, BNIP3 and LC3B changes during immobilization. (**E–H**) Statistics for the grey value analysis of western blotting bands for HIF-1α, Beclin-1, BNIP3 and LC3B (n = 6 per group). (**I**) Immunofluorescence assay was conducted to localize the co-expression of LC3B and BNIP3, which appeared in yellow. Scale bars = 50 μm. (**J**) Quantitative analysis of immunofluorescence assessing the co-localization of LC3B and BNIP3 was carried out (n = 6 per group). All values were presented as mean ± SD. ns, no significance. $*p < 0.05$, $**p < 0.01$, $***p < 0.001$, $****p < 0.0001$. DHE, dihydroethidium; SOD, superoxide dismutase.

(Abcam, ab11083, Shanghai, China; dilution 1:100) and rabbit polyclonal antibody against fast skeletal myosin (Abcam, ab228727, Shanghai, China; dilution 1:100). On additional slides, incubation of the rabbit polyclonal antibody against BNIP3 (ABclonal, A5683, Wuhan, China; dilution 1:100) with the mouse monoclonal antibody against LC3B (ABclonal, A17424, Wuhan, China; dilution 1:100) was carried out for 2 h at 37 °C. As a secondary antibody, FITC-conjugated Goat anti-Rabbit IgG (heavy chain + light chain (H + L)) (ABclonal, AS011, Wuhan, China; dilution 1:100) and Cy3-conjugated Goat anti-Mouse IgG (H + L) (ABclonal, AS008, Wuhan, China; dilution 1:100) were applied to the sections at 37 °C for 1 h following a wash with PBS. The sections were stained at room temperature for 5 min using 4',6-diamidino-2-phenylindole (DAPI) (Bey-

otime, C1005, Shanghai, China). A fluorescence microscope (Olympus, Tokyo, Japan, BX-51) with a field of view of 400× magnification was used to observe each section. In order to analyze the transition of myofiber type analysis, each section was analyzed with Image J (Image J v1.46a, National Institutes of Health, Bethesda, MD, USA) using three randomly selected fields of view, and the ratio of fast type fiber (green) to slow type fiber (red) in each visual field was calculated for statistical analysis. For each section, six random, noncontiguous microscopic fields were also analyzed using Image J in order to analyze co-localization between LC3B and BNIP3 (yellow puncta). Based on previous protocols, the mean number of yellow puncta in each visual field was counted for statistical analysis (Wang *et al.*, 2023b).
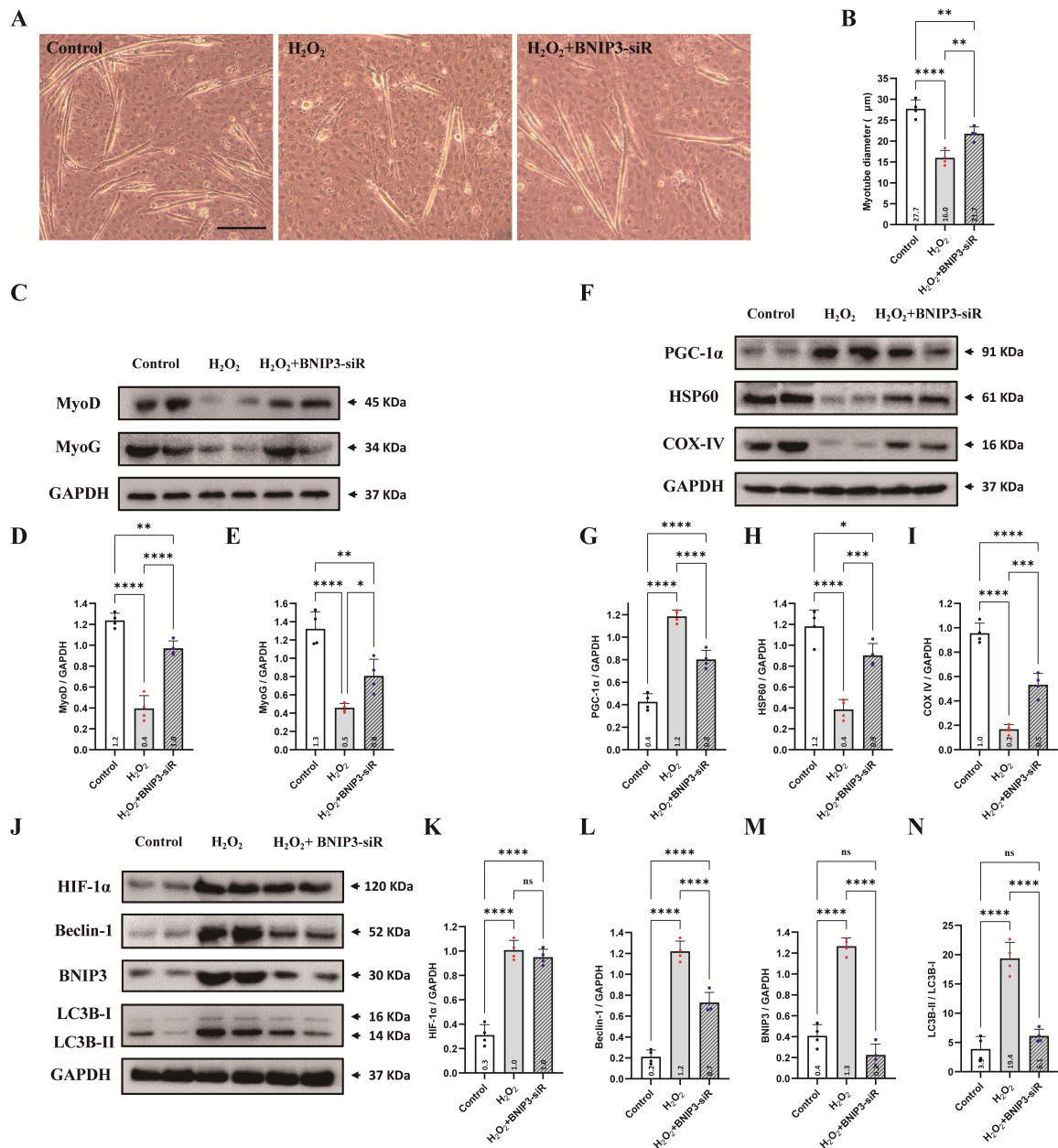
**Fig. 5. Myotube formation was inhibited due to hyperactive activation of ROS-mediated HIF-1α/BNIP3-dependent mitophagy in C2C12 myoblasts.** (**A**) Typical images of C2C12 murine myotubes photographed by inverted phase contrast microscopy to quantify the myotube diameter. Scale bars = 100 $\mu$m. (**B**) Quantitative analysis of the averaged diameter of myotubes (n = 4 per group). (**C**) Western blotting results showing MyoD and MyoG changes. (**D,E**) Statistics for the grey value analysis of western blotting bands for MyoD and MyoG (n = 4 per group). (**F**) Western blotting results showing PGC-1α, HSP60 and COX IV changes. (**G–I**) Statistics for the grey value analysis of western blotting bands for PGC-1α, HSP60 and COX IV (n = 4 per group). (**J**) Western blotting results showing HIF-1α, Beclin-1, BNIP3 and LC3B changes. (**K–N**) Statistics for the grey value analysis of western blotting bands for HIF-1α, Beclin-1, BNIP3 and LC3B (n = 4 per group). All values were presented as mean $\pm$ SD. ns, no significance. $*p < 0.05$, $**p < 0.01$, $***p < 0.001$, $****p < 0.0001$. MyoD, myogenic differentiation; MyoG, myogenin.

*Cell Culture and Differentiation*

According to the protocol in previous research (Chen *et al.*, 2021), C2C12 cells obtained from Procell (Procell Life Science & Technology Co., Ltd., CL-0044, Wuhan, China) were authenticated by short tandem repeat (STR) profiling and cultured in Dulbecco's modified Eagle's medium (DMEM) supplemented with fetal bovine serum (10 %), penicillin (100 IU/mL), and streptomycin (100 $\mu$g/mL). The cells were maintained at 37 °C in a 5 % $CO_2$ atmosphere with 95 % humidity. When the density of C2C12 cells was about 90 %, the cells were collected and then were assigned into group Control, group
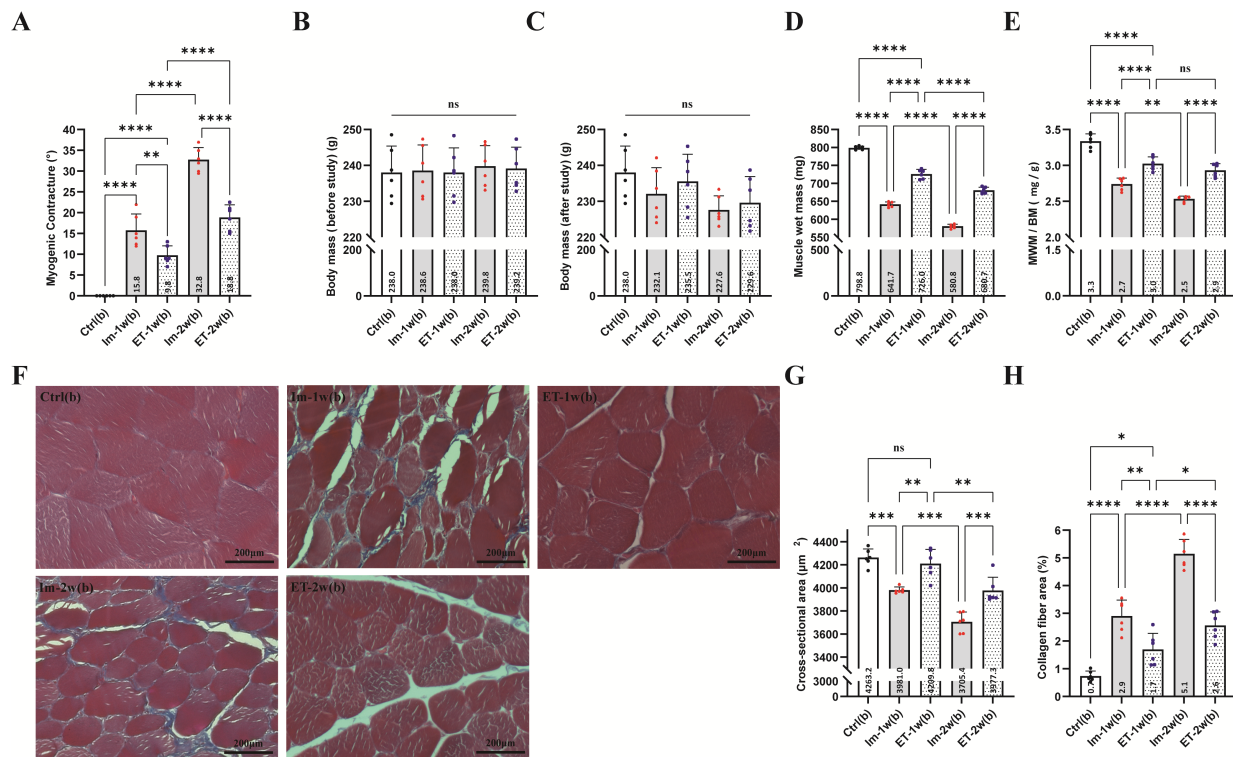
**Fig. 6. ESW delayed the development of immobilization-induced myogenic contracture and muscle atrophy.** (**A**) Statistical graphs of myogenic contracture (°) (n = 6 per group). (**B–E**) Statistical graphs of body mass (before study) (g), body mass (after study) (g), muscle wet mass of the rectus femoris (mg), and MWM/BM (mg/g) (n = 6 per group). (**F**) Typical Masson staining images. Scale bars = 200 $\mu$m. (**G,H**) Statistical graphs of cross-sectional area ($\mu$m$^2$), ratio of collagen fiber area to myofiber area (n = 6 per group). All values were presented as mean $\pm$ SD. ns, no significance. *$p < 0.05$, **$p < 0.01$, ***$p < 0.001$, ****$p < 0.0001$.

$H_2O_2$, and group $H_2O_2$+BNIP3-siR. In order to investigate whether high level ROS inhibited myoblast differentiation and activated HIF-1$\alpha$/BNIP3-dependent mitophagy, the C2C12 cells in $H_2O_2$ group were stimulated using 400 $\mu$M $H_2O_2$ for 8 h (Chen *et al.*, 2021). To investigate whether BNIP3-dependent mitophagy inhibits myoblast differentiation, C2C12 cells in group $H_2O_2$ + BNIP3-siR were pretreated with BNIP3 siRNA prior to $H_2O_2$ stimulation. Small interfering RNA (siRNA) targeting BNIP3 (BNIP3 siRNA) was obtained from Gene Pharma (Gene Pharma Ltd., Shanghai, China). The scrambled RNA (Gene Pharma Ltd., Shanghai, China) was used as vehicle control to confirm that the observed effects were specifically due to BNIP3 silencing and not due to off-target effects of siRNA transfection (**Supplementary Fig. 1**). The siRNA was transfected into the C2C12 cells according to the manufacturer's instructions, using Lipofectamine 2000 Transfection Reagent. The sequences for BNIP3 siRNA were as follows: 5′- GCAUCAAGUUACAGGUCUUTT-3′ (forward), 5′-AAGACCUGUAACUUGAUGCTT-3′ (reverse). The sequences for scrambled siRNA control were as follows: 5′-UUCUCCGAACGUGUCACGUTT-3′ (forward), 5′-ACGUGACACGUUCGGAGAATT-3′ (reverse). Subsequently, the cells were switched to differentiation medium (DM) containing horse serum (2 %), penicillin

(100 IU/mL), and streptomycin (100 $\mu$g/mL) in DMEM. In the subsequent five days, the medium was changed every other day. To evaluate the diameter of differentiated C2C12 myotubes, six random culture fields in each group were captured using an inverted phase-contrast microscopy (Nikon Ltd., TE2000-U, Tokyo, Japan). According to previous research (Miki *et al.*, 2019), the mean myotube diameter was calculated from the average diameter of at least 200 myotubes measured in each well using Image J software (Image J v1.46a, National Institutes of Health, Bethesda, MD, USA).

*Western Blot*

The total protein of rectus femoris samples and C2C12 cells were extracted using RIPA buffer (Beyotime, P0013E, Shanghai, China) containing protease and phosphatase inhibitor cocktail (Beyotime, P1049, Shanghai, China) at 4 °C. The protein concentration was determined using a Pierce BCA Protein Assay kit (Beyotime, P0012, Shanghai, China) in accordance with the manufacturer's instructions. After boiling the total protein, the proteins were separated using sodium dodecyl sulfate-polyacrylamide gel electrophoresis (SDS-PAGE) (8 %–15 %). Upon trimming the gels, the samples were transferred onto a polyvinylidene fluoride (PVDF) membrane in parallel and the gels/blots
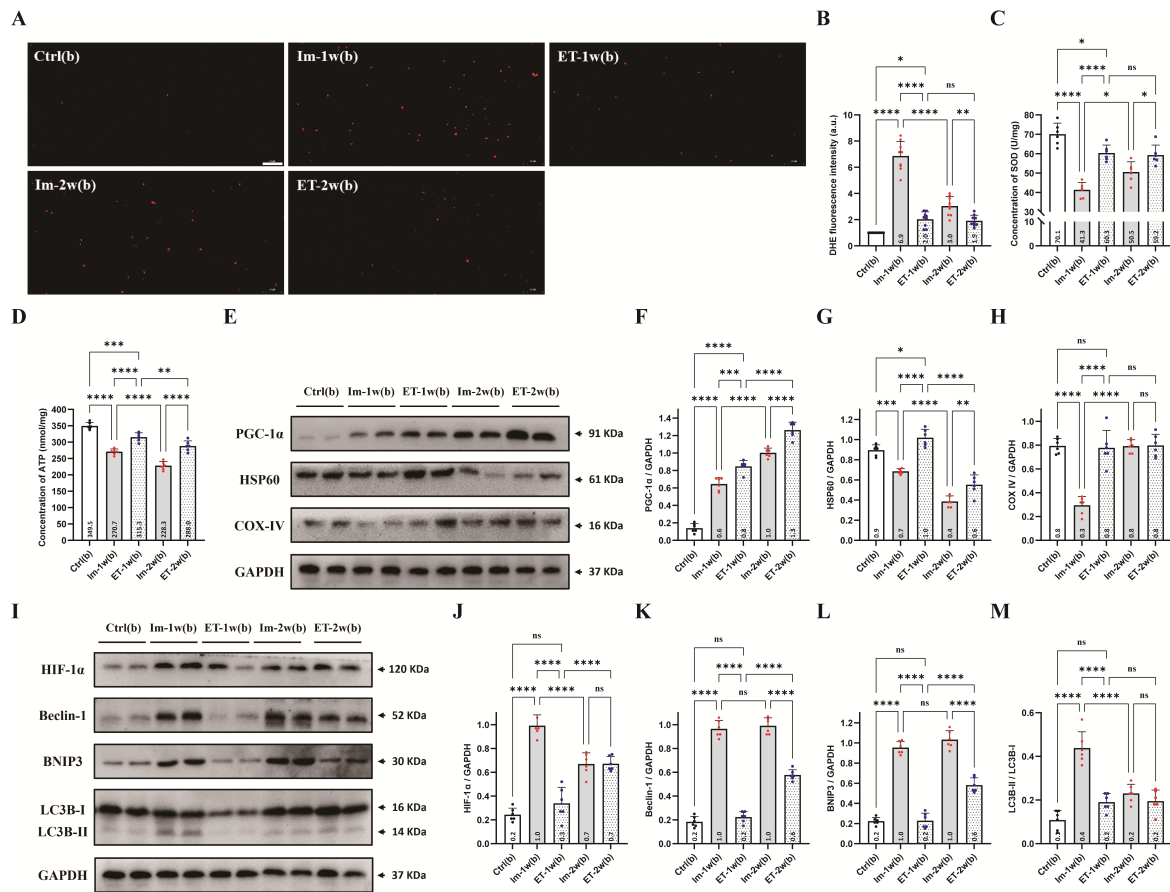
**Fig. 7. ESW reduced hyperactive activation of ROS-mediated HIF-1$\alpha$/BNIP3-dependent mitophagy during immobilization.** (**A**) Typical DHE fluorescence images to assess ROS generation. Scale bars = 50 $\mu$m. (**B**) DHE fluorescence intensity in each group was described as a percentage of group Ctrl(b) (n = 6 per group). (**C**) Statistical graphs of SOD level (U/mg) (n = 6 per group). (**D**) Statistical graphs of ATP level (nmol/mg) (n = 6 per group). (**E**) Western blotting results showing PGC-1$\alpha$, HSP60 and COX IV changes. (**F–H**) Statistics for the grey value analysis of western blotting bands for PGC-1$\alpha$, HSP60 and COX IV (n = 6 per group). (**I**) Western blotting results showing HIF-1$\alpha$, Beclin-1, BNIP3 and LC3B changes. (**J–M**) Statistics for the grey value analysis of western blotting bands for HIF-1$\alpha$, Beclin-1, BNIP3 and LC3B (n = 6 per group). All values were presented as mean $\pm$ SD. ns, no significance. *$p < 0.05$, **$p < 0.01$, ***$p < 0.001$, ****$p < 0.0001$.

originated from the same experiment. The membranes were blocked for 2 h at room temperature using five percent non-fat dry milk in Tris-buffered saline Tween-20 (TBST). Following this, the membranes were incubated at 4 °C overnight with primary antibody including rabbit monoclonal antibody against HIF-1$\alpha$ (Abcam, ab179483, Shanghai, China), rabbit polyclonal antibody against PGC-1$\alpha$ (ABclonal, A12348, Wuhan, China; dilution 1:1000), rabbit monoclonal antibody against HSP60 (Abcam, ab190828, Shanghai, China; dilution 1:1000), rabbit monoclonal antibody against COX IV (Abcam, ab202554, Shanghai, China; dilution 1:1000), rabbit monoclonal antibody against Beclin-1 (Abcam, ab210498, Shanghai, China; dilution 1:1000), rabbit polyclonal antibody against LC3B (Abcam, ab63817, Shanghai, China; dilution 1:2000), rabbit monoclonal antibody against MyoD (Abcam, ab133627, Shanghai, China; dilution 1:2000), and rabbit monoclonal antibody against myogenin (MyoG)

(Abcam, ab124800, Shanghai, China; dilution 1:2000). On the second day, membranes were incubated for 2 h at room temperature with peroxidase-conjugated Affinipure goat anti-rabbit IgG-horseradish peroxidase (HRP) (Abcam, ab6721, Shanghai, China; 1:5000 dilution) as the secondary antibody, following three 10-minute washes in TBST. After being washed three times with TBST or 10 min per wash, the membranes were evaluated with the enhanced chemiluminescence system in accordance with the manufacturer's instructions. The band densities were quantified using Image J software (Image J v1.46a, National Institutes of Health, Bethesda, MD, USA). The relative protein levels were calculated by comparison with the amount of Glyceraldehyde-3-phosphate Dehydrogenase (GAPDH) (Abcam, ab9485, Shanghai, China; dilution 1:1000) as a loading control. Each sample was run in triplicate and each western blot was repeated three times. The acquired values for each group were averaged for statistical analysis.

For each group, the means (standard deviations) of the results were shown. The statistical software Graph Pad Prism® Version 9.0.0 (Graph-Pad Software, San Diego, CA, USA) was used to conduct statistical analysis and create statistical graphs. In part a of animal experimental, one-way analysis of variance was used to compare the means of the groups, and Tukey's post hoc test was used when the data displayed a normal distribution. In part b of the animal experiment, the impact of ESW for each of the outcome measures was evaluated using two-way repeated measures analysis of variance. *In vitro* experimental, comparisons between groups were performed by using the unpaired *t*-test.

# Results

*Immobilization Caused Myogenic Contracture and Muscle Atrophy*

The content of myogenic contracture increased with the duration of immobilization. After three weeks of immobilization, the most notable increase was observed (Fig. 2**A**). However, no significant difference was found between group Im-2w(a) and group Im-3w(a) (Fig. 2**A**). The MWM and MWM/BM consistently decreased from the third day to the second week, indicating significant rectus femoris atrophy (Fig. 2**B–F**).

The most notable reduction in average CSA occurred after three weeks (Fig. 2**G,H**). However, there was no significant difference between group Im-2w(a) and group Im-3w(a) (Fig. 2**G,H**). Additionally, the ratio of collagen fiber area to myofiber area showed the most significant increase in group I-3w (Fig. 2**G,I**), but there was no significant difference between group Im-2w(a) and group Im-3w(a) (Fig. 2**G,I**). Immunofluorescence revealed the ratio of fast type fibers to slow type fibers increased significantly with longer immobilization periods, with the largest increase observed after three weeks (Fig. 2**J,K**).

*Mitophagy in Skeletal Muscle was Overactivated after Immobilization*

In the group Ctrl(a), morphology and number of mitochondria appeared generally normal. However, after only one day of immobilization, enlarged and swollen mitochondria were observed, and the cristae appeared disordered, disrupted, or absent. Mitophagosomes, which have a double-layered membrane and contain damaged mitochondria, were also observed. As the duration of immobilization increased, there was a significant accumulation of mitophagosomes, a large presence of vacuolated mitochondria, and a reduction in the overall number of mitochondria (Fig. 3**A**).

The results indicated a declining trend in total ATP content throughout the immobilization period (Fig. 3**B**). Furthermore, the expression level of COX IV protein decreased initially, followed by an increase with increasing immobilization time (Fig. 3**C,F**). Conversely, the level

of HSP60 protein showed a consistent decrease over the course of immobilization period (Fig. 3**C,E**). However, the expression level of PGC-1α was significantly elevated in response to immobilization (Fig. 3**C,D**).

*Immobilization Increased ROS Generation and Up-Regulated HIF-1α/BNIP3 Dependent Mitophagy*

During immobilization, a trend of increasing-decreasing fluorescence intensity was observed (Fig. 4**A,B**). Notably, the group Im-1w(a) displayed the most obvious increase in fluorescence intensity. Conversely, a subsequent decrease in fluorescence intensity was observed after the first week. Furthermore, the Im-3w group showed the most pronounced decrease in fluorescence intensity. Apart from this, a negative correlation was noted between the DHE fluorescence intensity and the concentration of SOD, with the most notable reduction in the concentration of SOD occurring in group Im-1w(a) compared to group Ctrl(a) (Fig. 4**C**).

The immobilization of subjects resulted in a trend of increasing and decreasing protein expression of HIF-1α (Fig. 4**D,E**). Notably, the Im-3d(a) group showed the most significant growth, although no significant difference emerged between Im-3d(a) and Im-1w(a) groups. BNIP3 expression peaked at two weeks and decreased by three weeks (Fig. 4**D,G**). The expression level of Beclin-1 continuously increased but subsequently dropped to a relatively lower level at three weeks (Fig. 4**D,F**). The LC3B-II/LC3B-I ratio increased after three days and remained at a heightened level until three weeks (Fig. 4**D,H**).

In present study, we utilized immunofluorescence analysis to examine the co-localization BNIP3 (green fluorescence-labeled) and LC3B (red fluorescence-labeled), as shown in **Supplementary Fig. 2**. We observed a gradual increase in the mean number of the co-localization of LC3B and BNIP3 (yellow fluorescence-labeled) within individual muscle fibers, with a peak at the second week (Fig. 4**I,J**).

*Myotube Formation was Inhibited due to Hyperactive Activation of ROS-Mediated HIF-1α/BNIP3-Dependent Mitophagy in C2C12 Myoblasts*

The results indicated that $H_2O_2$ stimulation resulted in a decrease in the average diameter of myotubes (Fig. 5**A,B**), along with a downregulation of the protein levels of MyoD and myogenin (MyoG) (Fig. 5**C–E**). The muscle regulatory factors (MRFs) family, which is secreted by satellite cells, includes MyoD, MyoG, myogenic factors 5 (Myf5), and muscle regulatory factor 4 (MRF4). Specifically, MyoD is involved early in myogenesis to determine myogenic fate, whereas MyoG plays a later role in the differentiation of myoblasts into myotubes. Moreover, we found that ROS-induced BNIP3 was significantly inhibited when BNIP3 was silenced by siRNA transfection (Fig. 5**C–N**). The reduction in mitophagy was correlated with the reduction in

BNIP3 protein level, as demonstrated in Fig. **5J,M**. Notably, the reduction in the averaged diameter of myotubes and the protein levels of MyoD and MyoG induced by $H_2O_2$ stimulation were partially reversed by BNIP3 siRNA transfection (Fig. **5C–E**).

### *ESW Inhibited the Development of Immobilization-Induced Myogenic Contracture and Muscle Atrophy*

As shown in Fig. **6A**, the myogenic contracture developed to varying degrees in both groups ET(b) and Im(b) during the two-week immobilization period. However, the myogenic contracture was markedly larger in groups Im(b) compared to groups ET(b) at the same instant.

As shown in Fig. **6B–E**, the Im(b) groups had a more significant reduction in MWM and MWM/BM when compared to the ET(b) groups at the same instant. Additionally, Masson-stained cross-sections revealed that the Im(b) groups had a more noticeable reduction in CSA when compared to the ET(b) groups (Fig. **6F,G**). Furthermore, the ratio of collagen fiber area to myofiber area rose at a considerably slower pace in the ET(b) groups when compared to the Im(b) groups throughout the immobilization period (Fig. **6F,H**).

### *ESW Reduced Overactivation of ROS-Mediated HIF-1α/BNIP3-Dependent Mitophagy during Immobilization*

As depicted in Fig. **7A,B**, our findings revealed a significant increase in DHE fluorescence intensity in both group ET-1w(b) and group Im-1w(b), as compared to group Ctrl(b). Notably, a significantly lower DHE fluorescence intensity was observed in group ET-1w(b) as compared to group Im-1w(b). In addition, while group Im-2w(b) exhibited a slight downregulation in DHE fluorescence intensity as compared to groups Im-1w(b), group ET-2w(b) demonstrated a far weaker DHE fluorescence intensity in comparison to groups Im-2w(b). Additionally, the activity of SOD in group ET(b) was significantly upregulated compared to group Im(b) at the same instant (Fig. **7C**).

Throughout the two-week immobilization period, the activation levels of HIF-1α/BNIP3-dependent mitophagy-related proteins, including HIF-1α, BNIP3, LC3B-II/LC3B-I ratio, and Beclin-1, were found to vary in both groups ET(b) and Im(b) (Fig. **7I–M**). However, while HIF-1α expression level and LC3B-II/LC3B-I ratio were comparable between the groups at the second week, the activation level of HIF-1α/BNIP3-dependent mitophagy was significantly lower in groups ET(b) as compared to groups Im(b) during the two-week immobilization period. Furthermore, ESW partially suppressed the reduction of mitochondrial markers like HSP60 and COX-IV (Fig. **7E,G,H**). In addition, ESW enhanced the expression of PGC-1α in a time-dependent manner (Fig. **7E,F**). These findings were confirmed by TEM analysis (**Supplementary Fig. 3**). Although the mitochondrial morphology and quantity in group ET-1w(b) and group ET-2w(b) were not as favorable as those in group Ctrl(b), they were significantly improved compared to groups Im(b) during the same immobilization period. Importantly, relatively few mitophagosome formations were observed by TEM in groups ET(b) as compared to groups Im(b) during the same immobilization period. Furthermore, the total ATP content in group ET(b) was significantly upregulated compared to group Im(b) at the same instant ($p < 0.05$, Fig. **7D**).

## Discussion

With the development of the transportation and construction industries, there is a rising number of patients requiring prolonged limb immobilization or bed rest due to trauma. This leads to muscle atrophy, which contributes to myogenic contracture and negatively affects the quality of life and social engagement, especially among the elderly. Therefore, it is essential to find a noninvasive treatment that can improve muscle atrophy. The involvement of mitophagy in muscle has gained recognition in recent years. However, it remains unclear whether mitophagy is the primary driver of muscle atrophy induced by immobilization, as upregulation of mitophagy can also be complementary to atrophic. Therefore, this study proposes to examine the relationship between BNIP3-dependent mitophagy and muscle atrophy in the context of myogenic contracture progression. Additionally, we aim to determine whether ESW can inhibit the development of immobilization-induced myogenic contracture by reducing BNIP3-dependent mitophagy in skeletal muscle.

Moderate physical activity is crucial for maintaining joint and muscle function. Our current findings support previous research, which demonstrated that immobilization leads to muscle atrophy and myofibrosis, resulting in knee joint myogenic contracture (Wang *et al.*, 2023a). Previous studies have shown that immobilization or unloading leads to a transition from slow to fast myofibers (Marino Gammazza *et al.*, 2018; Wang *et al.*, 2017). Our immunofluorescence results revealed a higher ratio of fast type fibers to slow type fibers after immobilization. These differences in muscle fiber type are associated with mitochondrial content and oxidative capacity. Slow type fibers have higher mitochondrial content and rely more on oxidative phosphorylation compared to fast type fibers (Grichko *et al.*, 2000). Mitochondria are essential for energy production in muscles, and proper mitochondrial function is crucial for ATP generation. Importantly, our results also indicated a decreasing trend in total ATP content during immobilization. Based on these findings, we hypothesize that immobilization-induced muscle atrophy is linked to mitochondrial dysfunction.

Previous research has demonstrated that significant atrophic stimuli, such as disuse and denervation, are associated with increased mitophagic signaling (Graham *et al.*, 2018; Zhang *et al.*, 2019). Furthermore, atrophied

muscle has been shown to have a reduction in mitochondrial quantity and quality (Borgia *et al.*, 2017; Kang *et al.*, 2016). Specifically, prior research using the mito-QC mitophagy reporter mouse indicated that soleus muscle atrophy was linked to increased expression of mitophagy-related genes following hindlimb immobilization (Yamashita *et al.*, 2021). In our study, we found that with an extension of immobilization duration, mitochondrial morphological abnormalities, overactivated mitophagy, and loss of mitochondrial quantity were observed by TEM. Our experiments further found that the significant reduction of mitochondrial proteins, particularly COX IV and HSP60, may be associated with the overactivated mitophagy rather than the inhibition of mitochondrial biogenesis. It is possible that enhancing the expression of PGC-1$\alpha$, a transcriptional co-activator encouraging mitochondrial biogenesis, may act as a compensatory protective mechanism during immobilization, as the expression level of COX IV almost returned to baseline levels at the end of immobilization. Previous research has reported that hind limb suspension led to increased receptor-mediated mitophagy and reduced regulation of mitochondrial biogenesis in the gastrocnemius of mice. However, no changes were observed in the protein and mRNA levels related to mitochondrial biogenesis during uploading in the vastus lateralis muscle of humans (Leermakers *et al.*, 2019). Different species, muscle types, immobilization times, and markers of mitochondria biogenesis may account for this discrepancy (Deval *et al.*, 2020).

It is widely accepted that mitochondria serve as the primary site of aerobic energy production, and that ROS, which are produced as a byproduct of mitochondrial metabolism, may promote HIF-1$\alpha$/BNIP3-dependent mitophagy. Within one week of immobilization, ROS generation and HIF-1$\alpha$ expression were enhanced, followed by downregulation. This is consistent with our expectation, as ROS induce mitophagy, a process that eliminates damaged mitochondria and controls ROS levels (Fu *et al.*, 2020). In the present study, we observed that the protein expression levels of BNIP3, LC3B-II/LC3B-I, and Beclin-1 were upregulated after immobilization, suggesting that HIF-1$\alpha$/BNIP3-dependent mitophagy was activated through the over-generation of ROS. The immunofluorescence analysis also provided additional proof for BNIP3-dependent mitophagy in atrophic muscle after immobilization. Additionally, our results showed that high levels of ROS inhibited myogenic differentiation in C2C12 cells and elevated the level of HIF-1$\alpha$/BNIP3-dependent mitophagy. Importantly, pretreatment with BNIP3 siRNA reduced the level of BNIP3-dependent mitophagy and partially counteracted the inhibition of myogenic differentiation caused by high levels of ROS in C2C12 cells. To our knowledge, this is the first investigation to provide detailed information about how mitophagy affects muscle atrophy throughout immobilization. These findings underscore the importance of studying the role of mitophagy in skeletal muscle func-

tion and the therapeutic potential of targeting mitophagy to prevent muscle atrophy. Notably, previous research revealed that BNIP3-dependent mitophagy also may require the translocation of Parkin to the mitochondria (Lee *et al.*, 2011). In contrast, a prior study found that the expression of PTEN induced putative kinase 1 (PINK1) and Parkin in rectus femoris remained stable between control and 2 weeks of immobilization (Wang *et al.*, 2023b). Additionally, previous research also demonstrated that immobilizing gastrocnemius for one week did not alter Parkin protein levels, but did raise BNIP3 mRNA levels. The proportions of muscle fiber types and their anatomical positioning may contribute to this phenomenon throughout immobilization (Deval *et al.*, 2020).

In this study, we investigated the therapeutic benefits of ESW during immobilization. Our results showed a quantifiable reduction in myogenic contracture and significant improvements in muscle atrophy, including MWW and CSA. Our results showed that myogenic contracture was smaller in groups ET(b) than in groups Im(b), and MWM/BM was greater in groups ET(b) than in groups Im(b) at the same instant. Our histological evaluation further corroborated these results. Interestingly, we found that CSA was reduced in both the Im(b) and ET(b) groups after the first week of immobilization, and this reduction progressed over time up to two weeks. However, ESW substantially reduced the development of CSA reduction. Our study also provides evidence that ESW can inhibit the development of muscle atrophy by ameliorating indicators associated with ROS generation, HIF-1$\alpha$/BNIP3-dependent mitophagy, and mitochondrial biogenesis. Previous publications have shown that ESW can reduce or inhibit the generation of ROS in the cardiovascular and nervous systems, supporting our findings (Graber *et al.*, 2022; Qiu *et al.*, 2021). As expected, ESW protected the destruction of mitochondrial structure and reduced the formation of mitophagosomes. Although the protein expression levels of BNIP3-dependent mitophagy were also up-regulated to some degree in groups ET(b) compared to groups Ctrl(b), we observed a far weaker activation effect for BNIP3-dependent mitophagy induced by immobilization after application with ESW. Interestingly, the protein expression of PGC-1$\alpha$ was further up-regulated in groups ET(b) compared to groups Im(b), indicating that ESW might play a role in mitochondrial biogenesis. Although the reason for this phenomenon remains to be clarified, previous research has reported that ESW can reverse ischemia-related ventricular remodeling and preserve ventricular function, accompanied by elevated mRNA expression of PGC-1$\alpha$ (Fu *et al.*, 2011).

This study has certain limitations. In consideration of animal ethics and welfare, we applied ice compress to a small number of rats that developed subcutaneous microhemorrhage. Previous research indicated that low temperature did not suppress muscle atrophy (Ikeda *et al.*, 2023; Nagano

and Hori, 2014). Previous study also showed that exposure to cold affects the lipid metabolism of skeletal muscle by triggering mitophagy through HIF-1$\alpha$ (Chen *et al.*, 2023). Overall, low temperature might be detrimental to mitochondrial function and recovery from skeletal muscle atrophy. We recognized that this is an unavoidable part of the experimental process that may have an impact on the results. However, the purpose of our study was to investigate the mechanisms behind the potential benefits of ESW in reducing muscle atrophy and myogenic contracture, and we considered that ice compress will not cause impact on our conclusions. The present study only evaluated the short-term therapeutic effects of ESW, without assessing its long-term efficacy and safety. Apart from this, due to the lack of standard guidelines, the optimal dosage of ESW was determined primarily using the manufacturer's instructions, clinical practices, and our prior experimental experience, without detailed explanation. Future research should also take into account the optimal frequency and pressure parameters. This study would have benefited from the use of HIF-1$\alpha$ gene knockout or a specific HIF-1$\alpha$ inhibitor to directly investigate the mechanism of action of ESW *in vivo*.

## Conclusions

In summary, the present study provides clear evidence that immobilization induces muscle atrophy through overactivation of BNIP3-dependent mitophagy. Immobilization leads to the generation of high levels of ROS in skeletal muscle, which further overactivates HIF-1$\alpha$/BNIP3-dependent mitophagy. Excessive mitophagy results in the elimination of mitochondria, leading to a shortage of ATP supply. As ATP homeostasis is crucial for maintaining muscle mass, the shortage of ATP supply results in reduced muscle mass and CSA, as well as slow-to-fast myofiber type transition. Excessive ROS generation inhibits myotube formation in C2C12 myoblasts, and pretreatment with BNIP3 siRNA can reduce the level of BNIP3-dependent mitophagy and partially counteracted the inhibition of myogenic differentiation caused by high levels of ROS. Thus, inhibition of ROS generation and BNIP3-dependent mitophagy activation can prevent the development of immobilization-induced muscle atrophy. Based on these findings, the present study also demonstrates that ESW can inhibit overactivated ROS-mediated HIF-1$\alpha$/BNIP3-dependent mitophagy in immobilized muscles, which could be one of the potential therapeutic mechanisms attenuating immobilization-induced muscle atrophy and further improving myogenic contracture.

## List of Abbreviations

ESW, extracorporeal shock wave; ROS, reactive oxygen species; BNIP3, Bcl2/adenovirus E1B 19kDa protein-interacting protein 3; HIF, hypoxia-inducible factor; LC3, microtubule-associated protein 1 light chain 3; MyoD, myogenic differentiation; ROM, range of motion; MWM, muscle wet mass; BM, body mass; MWM/BM, the ratio of muscle wet mass to body mass; CSA, cross-sectional area; PBS, phosphate buffered saline; TEM, transmission electron microscope; ATP, adenosine triphosphate; DHE, dihydroethidium; SOD, superoxide dismutase; DMEM, Dulbecco's modified Eagle's medium; STR, short tandem repeat; siRNA, small interfering RNA; DM, differentiation medium; TBST, Tris-buffered saline Tween-20; MyoG, myogenin; Myf5, myogenic factors 5; MRF4, muscle regulatory factor 4; PINK1, PTEN induced putative kinase 1; SD, standard deviation; ARNT, aryl hydrocarbon receptor nuclear translocator; HRE, hypoxia response element; ESWT, extracorporeal shock wave therapy; H + L, heavy chain + light chain; DAPI, 4',6-diamidino-2-phenylindole; SDS-PAGE, sodium dodecyl sulfate-polyacrylamide gel electrophoresis; PVDF, polyvinylidene fluoride; HRP, horseradish peroxidase; GAPDH, Glyceraldehyde-3-phosphate Dehydrogenase.

## Availability of Data and Materials

The datasets used and analyzed during the current study are available from the first author on reasonable request. All data generated or analyzed during this study are included in this published article. The manuscript, including related data, figures and tables, has not been previously published and are not under consideration elsewhere.

## Author Contributions

FW conceived the study, participated in its design and coordination, drafted and revised the manuscript, and performed vivo and vitro experiments. CXZ and TZ assisted with animal management, and helped perform animal experiments. LYN and QBZ analyzed the data, and assisted in the drafting and revising of the manuscript. YZ participated in the design, guided FW to draft the manuscript, and reviewed the final manuscript. All authors read and approved the final manuscript. All authors agreed to be accountable for all aspects of the work in ensuring that questions related to the accuracy or integrity of any part of the work were appropriately investigated and resolved.

## Ethics Approval and Consent to Participate

The experimental procedures and the animal use and care protocols were approved by the Institutional Animal Care and Use Committee of Anhui Medical University (LLSC20221126). The study was carried out in compliance with the ARRIVE Guidelines and the National Institutes of Health Guide for the use and care of laboratory animals. This work was performed at the Second Affiliated Hospital of Anhui Medical University.

## Acknowledgments

## Conflict of Interest

None of the authors have any conflicts of interest to disclose. All authors declare that the research was conducted in the absence of any commercial or financial relationships that could be a potential conflict of interest.

## Supplementary Material

Supplementary material associated with this article can be found, in the online version, at https://doi.org/10.22203/eCM.v048a11.

## References

Bar-Shai M, Carmeli E, Ljubuncic P, Reznick AZ (2008) Exercise and immobilization in aging animals: the involvement of oxidative stress and NF-kappaB activation. Free Radical Biology & Medicine 44: 202-214. DOI: 10.1016/j.freeradbiomed.2007.03.019.

Borgia D, Malena A, Spinazzi M, Desbats MA, Salviati L, Russell AP, Miotto G, Tosatto L, Pegoraro E, Sorarù G, Pennuto M, Vergani L (2017) Increased mitophagy in the skeletal muscle of spinal and bulbar muscular atrophy patients. Human Molecular Genetics 26: 1087-1103. DOI: 10.1093/hmg/ddx019.

Chen J, Sun Y, Huang S, Shen H, Chen Y (2021) Grub polypeptide extracts protect against oxidative stress through the NRF2-ARE signaling pathway. Animal Cells and Systems 25: 405-415. DOI: 10.1080/19768354.2021.2018043.

Chen W, Xu Z, You W, Zhou Y, Wang L, Huang Y, Shan T (2023) Cold exposure alters lipid metabolism of skeletal muscle through HIF-1$\alpha$-induced mitophagy. BMC Biology 21: 27. DOI: 10.1186/s12915-023-01514-4.

Deval C, Calonne J, Coudy-Gandilhon C, Vazeille E, Bechet D, Polge C, Taillandier D, Attaix D, Combaret L (2020) Mitophagy and mitochondria biogenesis are differentially induced in rat skeletal muscles during immobilization and/or remobilization. International Journal of Molecular Sciences 21: 3691. DOI: 10.3390/ijms21103691.

Fu M, Sun CK, Lin YC, Wang CJ, Wu CJ, Ko SF, Chua S, Sheu JJ, Chiang CH, Shao PL, Leu S, Yip HK (2011) Extracorporeal shock wave therapy reverses ischemia-related left ventricular dysfunction and remodeling: molecular-cellular and functional assessment. PLoS One 6: e24342. DOI: 10.1371/journal.pone.0024342.

Fu ZJ, Wang ZY, Xu L, Chen XH, Li XX, Liao WT, Ma HK, Jiang MD, Xu TT, Xu J, Shen Y, Song B, Gao PJ, Han WQ, Zhang W (2020) HIF-1$\alpha$-BNIP3-mediated mitophagy in tubular cells protects against renal ischemia/reperfusion injury. Redox Biology 36: 101671. DOI: 10.1016/j.redox.2020.101671.

Graber M, Nägele F, Röhrs BT, Hirsch J, Pölzl L, Moriggl B, Mayr A, Troger F, Kirchmair E, Wagner JF, Nowosielski M, Mayer L, Voelkl J, Tancevski I, Meyer D, Grimm M, Knoflach M, Holfeld J, Gollmann-Tepeköylü C (2022) Prevention of oxidative damage in spinal cord ischemia upon aortic surgery: first-in-human results of shock wave therapy prove safety and feasibility. Journal of the American Heart Association 11: e026076. DOI: 10.1161/jaha.122.026076.

Graham ZA, Harlow L, Bauman WA, Cardozo CP (2018) Alterations in mitochondrial fission, fusion, and mitophagic protein expression in the gastrocnemius of mice after a sciatic nerve transection. Muscle & Nerve 58: 592-599. DOI: 10.1002/mus.26197.

Grichko VP, Heywood-Cooksey A, Kidd KR, Fitts RH (2000) Substrate profile in rat soleus muscle fibers after hindlimb unloading and fatigue. Journal of Applied Physiology 88: 473-478. DOI: 10.1152/jappl.2000.88.2.473.

Huang HM, Li XL, Tu SQ, Chen XF, Lu CC, Jiang LH (2016) Effects of roughly focused extracorporeal shock waves therapy on the expressions of bone morphogenetic protein-2 and osteoprotegerin in osteoporotic fracture in rats. Chinese Medical Journal 129: 2567-2575. DOI: 10.4103/0366-6999.192776.

Ikeda D, Fujita S, Toda K, Yaginuma Y, Kan-No N, Watabe S (2023) Cold-induced muscle atrophy in zebrafish: Insights from swimming activity and gene expression analysis. Biochemistry and Biophysics Reports 36: 101570. DOI: 10.1016/j.bbrep.2023.101570.

Kaneguchi A, Ozawa J, Moriyama H, Yamaoka K (2017) Nociception contributes to the formation of myogenic contracture in the early phase of adjuvant-induced arthritis in a rat knee. Journal of Orthopaedic Research: Official Publication of the Orthopaedic Research Society 35:

1404-1413. DOI: 10.1002/jor.23412.

Kang C, Ji LL (2013) Muscle immobilization and remobilization downregulates PGC-1$\alpha$ signaling and the mitochondrial biogenesis pathway. Journal of Applied Physiology 115: 1618-1625. DOI: 10.1152/japplphysiol.01354.2012.

Kang C, Yeo D, Ji LL (2016) Muscle immobilization activates mitophagy and disrupts mitochondrial dynamics in mice. Acta Physiologica 218: 188-197. DOI: 10.1111/apha.12690.

Lee Y, Lee HY, Hanna RA, Gustafsson ÅB (2011) Mitochondrial autophagy by Bnip3 involves Drp1-mediated mitochondrial fission and recruitment of Parkin in cardiac myocytes. American Journal of Physiology. Heart and Circulatory Physiology 301: H1924-H1931. DOI: 10.1152/ajpheart.00368.2011.

Leermakers PA, Kneppers AEM, Schols AMWJ, Kelders MCJM, de Theije CC, Verdijk LB, van Loon LJC, Langen RCJ, Gosker HR (2019) Skeletal muscle unloading results in increased mitophagy and decreased mitochondrial biogenesis regulation. Muscle Nerve 60: 769-778. DOI: 10.1002/mus.26702.

Li XM, Wang K, Liu M, Zhang QB, Zhou Y (2024) Nicorandil mitigates arthrogenic contracture induced by knee joint extension immobilization in rats: interference with RhoA/ROCK signaling and TGF-$\beta$1/Smad pathway. European Cells & Materials 47: 59-72. DOI: 10.22203/eCM.v047a05.

Liu AY, Zhang QB, Zhu HL, Xiong YW, Wang F, Huang PP, Xu QY, Zhong HZ, Wang H, Zhou Y (2022) Low-frequency electrical stimulation alleviates immobilization-evoked disuse muscle atrophy by repressing autophagy in skeletal muscle of rabbits. BMC Musculoskeletal Disorders 23: 398. DOI: 10.1186/s12891-022-05350-5.

Marino Gammazza A, Macaluso F, Di Felice V, Cappello F, Barone R (2018) Hsp60 in skeletal muscle fiber biogenesis and homeostasis: from physical exercise to skeletal muscle pathology. Cells 7: 224. DOI: 10.3390/cells7120224.

Miki Y, Morioka T, Shioi A, Fujimoto K, Sakura T, Uedono H, Kakutani Y, Ochi A, Mori K, Shoji T, Emoto M, Inaba M (2019) Oncostatin M induces C2C12 myotube atrophy by modulating muscle differentiation and degradation. Biochemical and Biophysical Research Communications 516: 951-956. DOI: 10.1016/j.bbrc.2019.06.143.

Nagano K, Hori H (2014) Promotion of apoptosis and cytochrome c depletion by a low-temperature environment in hindlimb-unloading rats. Journal of Musculoskeletal & Neuronal Interactions 14: 464-472.

Oost LJ, Kustermann M, Armani A, Blaauw B, Romanello V (2019) Fibroblast growth factor 21 controls mitophagy and muscle mass. Journal of Cachexia, Sarcopenia and Muscle 10: 630-642. DOI: 10.1002/jcsm.12409.

Ou HC, Chu PM, Huang YT, Cheng HC, Chou WC, Yang HL, Chen HI, Tsai KL (2021) Low-level laser prevents doxorubicin-induced skeletal muscle atrophy by modulating AMPK/SIRT1/PCG-1$\alpha$-mediated mitochondrial function, apoptosis and up-regulation of pro-inflammatory responses. Cell & Bioscience 11: 200. DOI: 10.1186/s13578-021-00719-w.

Park S, Shin MG, Kim JR, Park SY (2019) Beta-lapachone attenuates immobilization-induced skeletal muscle atrophy in mice. Experimental Gerontology 126: 110711. DOI: 10.1016/j.exger.2019.110711.

Qiu Q, Shen T, Yu X, Jia N, Zhu K, Wang Q, Liu B, He Q (2021) Cardiac shock wave therapy alleviates hypoxia/reoxygenation-induced myocardial necroptosis by modulating autophagy. BioMed Research International 2021: 8880179. DOI: 10.1155/2021/8880179.

Qiu YN, Wang GH, Zhou F, Hao JJ, Tian L, Guan LF, Geng XK, Ding YC, Wu HW, Zhang KZ (2019) PM2.5 induces liver fibrosis via triggering ROS-mediated mitophagy. Ecotoxicology and Environmental Safety 167: 178-187. DOI: 10.1016/j.ecoenv.2018.08.050.

Scicchitano BM, Pelosi L, Sica G, Musarò A (2018) The physiopathologic role of oxidative stress in skeletal muscle. Mechanisms of Ageing and Development 170: 37-44. DOI: 10.1016/j.mad.2017.08.009.

Talbert EE, Smuder AJ, Min K, Kwon OS, Szeto HH, Powers SK (2013) Immobilization-induced activation of key proteolytic systems in skeletal muscles is prevented by a mitochondria-targeted antioxidant. Journal of Applied Physiology 115: 529-538. DOI: 10.1152/japplphysiol.00471.2013.

Wang D, Yang Y, Zou X, Zhang J, Zheng Z, Wang Z (2020a) Antioxidant apigenin relieves age-related muscle atrophy by inhibiting oxidative stress and hyperactive mitophagy and apoptosis in skeletal muscle of mice. The Journals of Gerontology. Series A, Biological Sciences and Medical Sciences 75: 2081-2088. DOI: 10.1093/gerona/glaa214.

Wang F, Han J, Wang X, Liu Y, Zhang Z (2022a) Roles of HIF-1$\alpha$/BNIP3 mediated mitophagy in mitochondrial dysfunction of letrozole-induced PCOS rats. Journal of Molecular Histology 53: 833-842. DOI: 10.1007/s10735-022-10096-4.

Wang F, Li W, Zhou Y, Huang PP, Zhang QB (2022b) Radial extracorporeal shock wave reduces myogenic contracture and muscle atrophy via inhibiting NF-$\kappa$B/HIF-1$\alpha$ signaling pathway in rabbit. Connective Tissue Research 63: 298-307. DOI: 10.1080/03008207.2021.1920934.

Wang F, Zhang QB, Zhou Y, Liu AY, Huang PP, Liu Y (2020b) Effect of ultrashort wave treatment on joint dysfunction and muscle atrophy in a rabbit model of extending knee joint contracture: Enhanced expression of myogenic differentiation. The Knee 27: 795-802. DOI: 10.1016/j.knee.2020.02.013.

Wang F, Zhou CX, Zheng Z, Li DJ, Li W, Zhou Y (2023a) Metformin reduces myogenic contracture and

myofibrosis induced by rat knee joint immobilization via AMPK-mediated inhibition of TGF-$\beta$1/Smad signaling pathway. Connective Tissue Research 64: 26-39. DOI: 10.1080/03008207.2022.2088365.

Wang F, Zhou T, Zhou CX, Zhang QB, Wang H, Zhou Y (2023b) The worsening of skeletal muscle atrophy induced by immobilization at the early stage of remobilization correlates with BNIP3-dependent mitophagy. BMC Musculoskeletal Disorders 24: 632. DOI: 10.1186/s12891-023-06759-2.

Wang J, Wang F, Zhang P, Liu H, He J, Zhang C, Fan M, Chen X (2017) PGC-1$\alpha$ over-expression suppresses the skeletal muscle atrophy and myofiber-type composition during hindlimb unloading. Bioscience, Biotechnology, and Biochemistry 81: 500-513. DOI: 10.1080/09168451.2016.1254531.

Wang K, Chen YS, Chien HW, Chiou HL, Yang SF, Hsieh YH (2022c) Melatonin inhibits NaIO$_3$-induced ARPE-19 cell apoptosis via suppression of HIF-1$\alpha$/BNIP3-LC3B/mitophagy signaling. Cell & Bioscience 12: 133. DOI: 10.1186/s13578-022-00879-3.

Yamashita SI, Kyuuma M, Inoue K, Hata Y, Kawada R, Yamabi M, Fujii Y, Sakagami J, Fukuda T, Furukawa K, Tsukamoto S, Kanki T (2021) Mitophagy reporter mouse analysis reveals increased mitophagy activity in disuse-induced muscle atrophy. Journal of Cellular Physiology 236: 7612-7624. DOI: 10.1002/jcp.30404.

Yang X, Xue P, Chen H, Yuan M, Kang Y, Duscher D, Machens HG, Chen Z (2020) Denervation drives skeletal muscle atrophy and induces mitochondrial dysfunction, mitophagy and apoptosis via miR-142a-5p/MFN1 axis. Theranostics 10: 1415-1432. DOI: 10.7150/thno.40857.

Yuan H, Wang K, Zhang QB, Wang F, Zhou Y (2023) The effect of extracorporeal shock wave on joint capsule fibrosis based on A$_2$AR-Nrf2/HO-1 pathway in a rat extending knee immobilization model. Journal of Orthopaedic Surgery and Research 18: 930. DOI: 10.1186/s13018-023-04420-1.

Zhang Y, Yu B, Yu J, Zheng P, Huang Z, Luo Y, Luo J, Mao X, Yan H, He J, Chen D (2019) Butyrate promotes slow-twitch myofiber formation and mitochondrial biogenesis in finishing pigs via inducing specific microRNAs and PGC-1$\alpha$ expression1. Journal of Animal Science 97: 3180-3192. DOI: 10.1093/jas/skz187.

Zhu HL, Shi XT, Xu XF, Zhou GX, Xiong YW, Yi SJ, Liu WB, Dai LM, Cao XL, Xu DX, Wang H (2021) Melatonin protects against environmental stress-induced fetal growth restriction via suppressing ROS-mediated GCN2/ATF4/BNIP3-dependent mitophagy in placental trophoblasts. Redox Biology 40: 101854. DOI: 10.1016/j.redox.2021.101854.

Zissler A, Steinbacher P, Zimmermann R, Pittner S, Stoiber W, Bathke AC, Sänger AM (2017) Extracorporeal shock wave therapy accelerates regeneration after acute skeletal muscle injury. The American Journal of Sports Medicine 45: 676-684. DOI: 10.1177/0363546516668622.

**Editor's note**: The Scientific Editor responsible for this paper was Kaili Lin.